Copyright © 1984, by the author(s).
All rights reserved.

Permission to make digital or hard copies of all or part of this work for personal or classroom use is granted without fee provided that copies are not made or distributed for profit or commercial advantage and that copies bear this notice and the full citation on the first page. To copy otherwise, to republish, to post on servers or to redistribute to lists, requires prior specific permission.

APPLICATION OF NONLINEAR CONSTANTS OF MOTION IN A SINGLE ELECTROMAGNETIC WAVE TO THE STUDY OF THE ALFVÉN-ION-CYCLOTRON INSTABILITY

by

Niels F. Ontani

Memorandum No. UCB/ERL M84/49

16 July 1984

ELECTRONICS RESEARCH LABORATORY

College of Engineering
University of California, Berkeley
94720

ERL Report No. M84/49
July 16, 1984

Application of Nonlinear Constants of Motion in a Single Electromagnetic Wave to the Study of the Alfvén-Ion-Cyclotron Instability

Niels F. Otani
Electronics Research Laboratory,
University of California, Berkeley, California 94720

ABSTRACT

Constants of motion are derived for particles moving in a single, circularly-polarized electromagnetic wave of arbitrary time-dependence propagating parallel to a uniform background magnetic field. The constant associated with helical symmetry is shown to restrict the particle motion to a very narrow region of velocity space. Features of the slow time-scale motion of fixed points associated with the existence of a fourth adiabatic invariant are described for the case of a slowly varying wave. Characteristics of the particle motion thus derived are applied to the analysis of 1d-3v simulations of the saturation of the Alfvén-ion-cyclotron (AIC) instability for a single wave. In particular, an explanation is offered for the appearence of a sharp edge in the velocity distribution function observed in the simulation.

I. INTRODUCTION

We have been considering in some detail the nonlinear behavior of particles in a single electromagnetic wave as part of our investigation of the single-wave saturation properties of the Alfvén-ion-cyclotron (AIC) instability. The system of fields used in this study are

$$\Omega_z = \Omega = \text{const}, \tag{1a}$$

$$\Omega_x = \Omega_1(t)\cos(kz - \varsigma(t)), \tag{1b}$$

$$\Omega_y = \Omega_1(t)\sin(kz - \varsigma(t)), \tag{1c}$$

$$\hat{\mathbf{z}} \times \frac{\partial \mathbf{E}}{\partial z} = -\frac{1}{c}\frac{\partial \mathbf{B}}{\partial t}, \tag{1d}$$

$$E_z = 0, \tag{1e}$$

$$\int_{z_0}^{z_0+2\pi/k} \mathbf{E}dz = 0, \tag{1f}$$

where $\Omega_{x,y,z} \equiv qB_{x,y,z}/mc$, z_0 is arbitrary, and $\Omega_1(t)$ and $\varsigma(t)$ are entirely arbitrary functions of t. These fields are characteristic of a single circularly-polarized, purely transverse electromagnetic wave propagating parallel to a uniform magnetic field. In the analysis, we first find constants of the particle motion in fields described by Eqs. (1) (Sec. II) and show these constants do much to characterize the nature of the particle orbits (Sec. III). Results of the analysis are then compared with, and applied to, self-consistent, single-wave particle simulations of the AIC instability (Sec. IV). Finally, conclusions are presented (Sec. V). Deserving of some emphasis is the fact that no assumptions will be made with respect to the magnitude or time-variation of the functions $\Omega_1(t)$ and $\varsigma(t)$ for many of the results presented. In particular, the wave amplitude need not be small and the time-variation of either the amplitude or the frequency of the wave need not be slow compared to a wave period. Thus application of the results is not limited to the study of the AIC instability; the theory will be valid for any wave satisfying Eqs. (1). The analysis should be relevant to monochromatic whistlers for example, on which much of the previous work on this wave structure has focused.[1-5]

II. THE CONSTANTS OF MOTION

We first show that, in spite of the generality of the fields' specifications, three exact constants of the particle motion exist. The constants are a direct consequence of the spatial symmetries of the system; specifically, (1) the system is invariant with respect to spatial translation in either the $\hat{\mathbf{x}}$- or $\hat{\mathbf{y}}$-directions, and (2) the system is also left unchanged under the combination of spatial translation along, and spatial rotation about, the $\hat{\mathbf{z}}$-axis, corresponding to the helical structure of the circularly-polarized wave.

With these symmetries in hand, standard Hamiltonian formulation easily reveals the corresponding constants. The Hamiltonian for this system is

$$H = \frac{1}{2}\left(\mathbf{p} - \frac{q}{mc}\mathbf{A}(\mathbf{x},t)\right)^2, \tag{2}$$

where $\mathbf{p} \equiv \mathbf{v} + q\mathbf{A}(\mathbf{x},t)/mc$, $\mathbf{v}$ is the particle velocity, $\mathbf{A}(\mathbf{x},t)$ is the vector potential, and the usual scalar potential $\phi(\mathbf{x},t)$ is chosen here to be identically zero.

Choosing as the vector potential

$$\frac{qA_x}{mc} = -y\Omega - \frac{\Omega_x(z,t)}{k}, \qquad \frac{qA_y}{mc} = -\frac{\Omega_y(z,t)}{k}, \qquad A_z = 0, \tag{3}$$

where $\Omega_x(z,t)$ and $\Omega_y(z,t)$ are given by Eqs. (1b) and (1c), we observe that H does not depend on x; consequently, the conjugate momentum $p_x = v_x - y\Omega - \Omega_x(z,t)/k$ is a conserved quantity. A constant of the motion may then be defined:

$$Y \equiv y - \frac{v_x}{\Omega} + \frac{\Omega_x(z,t)}{k\Omega}, \tag{4}$$

which reduces to the y-coordinate of the gyrocenter in the absence of the wave. Similarly, using for the vector potential

$$\frac{qA_x}{mc} = -\frac{\Omega_x(z,t)}{k}, \qquad \frac{qA_y}{mc} = x\Omega - \frac{\Omega_y(z,t)}{k}, \qquad A_z = 0, \tag{5}$$

we now find H cyclic in y. This leads to the other gyrocenter-like constant of motion

$$X \equiv x + \frac{v_y}{\Omega} - \frac{\Omega_y(z,t)}{k\Omega}. \tag{6}$$

The constant of motion corresponding to the spatial helical symmetry of the system may be derived by writing the vector potential as

$$\frac{qA_x}{mc} = -\tfrac{1}{2}y\Omega - \frac{\Omega_x(z,t)}{k}, \qquad \frac{qA_y}{mc} = \tfrac{1}{2}x\Omega - \frac{\Omega_y(z,t)}{k}, \qquad A_z = 0, \tag{7}$$

and substituting these expressions into the Hamiltonian Eq. (2):

$$H = \frac{p_z^2}{2} + \frac{1}{2}\left(p_x + \frac{y\Omega}{2} + \frac{\Omega_x(z,t)}{k}\right)^2 + \frac{1}{2}\left(p_y - \frac{x\Omega}{2} + \frac{\Omega_y(z,t)}{k}\right)^2. \tag{8}$$

A canonical transformation is then defined via the generating function[6]

$$F_2(x,y,z,P_\rho,P_{\theta_0},P_Z) = (x^2+y^2)^{1/2}P_\rho + \left(\tan^{-1}\frac{y}{x} - kz\right)P_{\theta_0} + zP_Z. \tag{9}$$

Taking partial derivatives of F_2 with respect to the new momenta P_ρ, P_{θ_0}, and P_Z yields the spatial part of the transformation:

$$\rho = (x^2+y^2)^{1/2}, \tag{10a}$$

$$\theta_0 = \tan^{-1}\frac{y}{x} - kz, \tag{10b}$$

$$Z = z. \tag{10c}$$

For reference, we give the inversions of Eqs. (10):

$$x = \rho\cos(\theta_0 + kZ), \tag{11a}$$

$$y = \rho\sin(\theta_0 + kZ), \tag{11b}$$

$$z = Z. \tag{11c}$$

Equations (10) define a helical coordinate system depicted schematically in Fig. 1. The coordinate system labels each point in space according to which helix passes through it (labeled by ρ and θ_0) and where along the helix it is located (labeled by Z). Each helix is labeled according to its point of intersection with the $z = 0$ plane. The polar coordinate

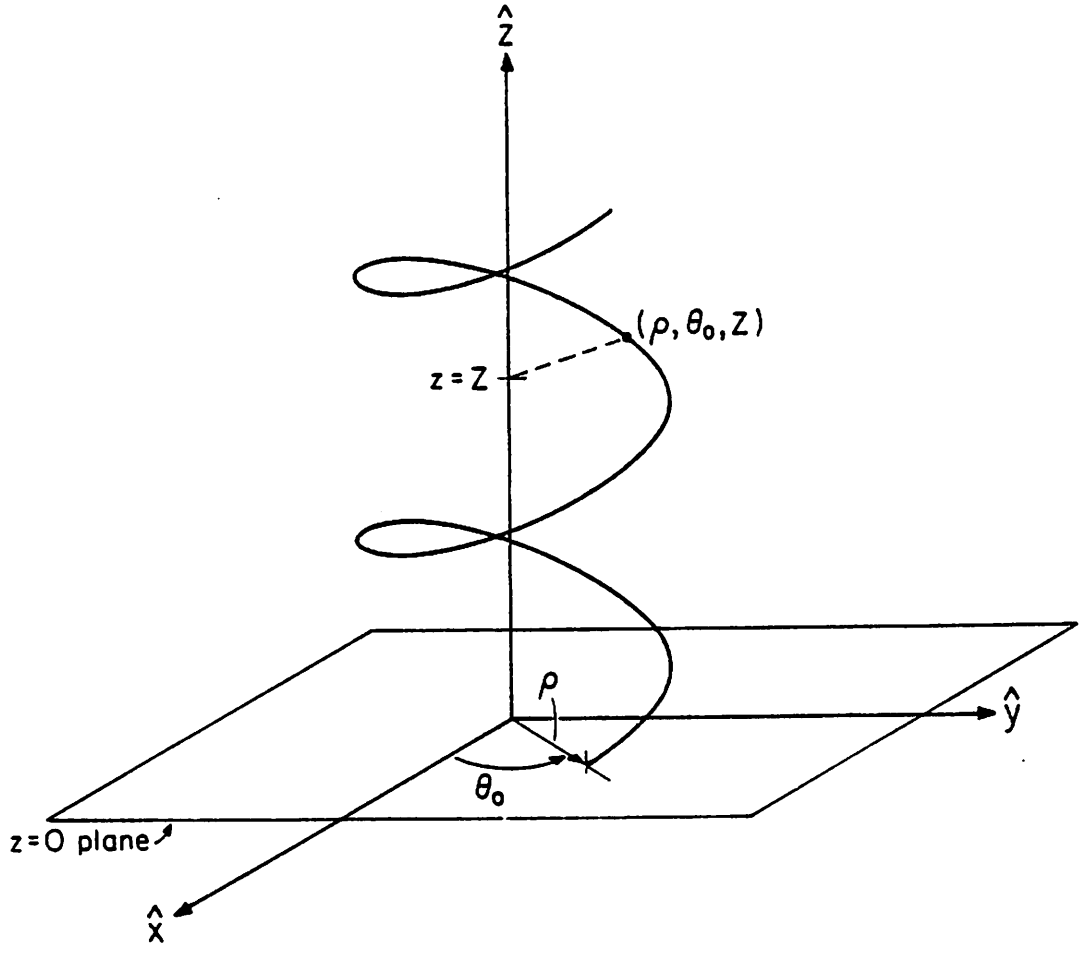

FIG. 1. Illustration of the (ρ, θ_0, Z) coordinate system. All points along a given helix have the same ρ- and θ_0-coordinates as determined by the intersection of the helix with the $z = 0$ plane, while the Z-coordinate of a given point is simply its height above the plane.

pair (ρ, θ_0) is used in describing this point as shown in Fig. 1. The location Z of a point along a given helix (ρ, θ_0) is specified simply by its old z-coordinate. By taking partial derivatives of F_2 with respect to the old coordinates x, y, and z and using Eqs. (11), we obtain the momentum portion of the transformation:

$$p_x = P_\rho \cos(\theta_0 + kZ) - \frac{P_{\theta_0}}{\rho} \sin(\theta_0 + kZ), \tag{12a}$$

$$p_y = P_\rho \sin(\theta_0 + kZ) + \frac{P_{\theta_0}}{\rho} \cos(\theta_0 + kZ), \tag{12b}$$

$$p_z = P_Z - kP_{\theta_0}. \tag{12c}$$

Equations (12) are easily inverted:

$$\rho P_\rho = xp_x + yp_y, \tag{13a}$$

$$P_{\theta_0} = xp_y - yp_x, \tag{13b}$$

$$P_Z = p_z + k(xp_y - yp_x). \tag{13c}$$

The canonical transformation may now be applied to the Hamiltonian H using Eqs. (11) and (12). Substituting explicit expressions for $\Omega_x(z,t)$ and $\Omega_y(z,t)$ from Eqs. (1), we obtain

$$\begin{aligned} H =& \tfrac{1}{2}(P_Z - kP_{\theta_0})^2 + \tfrac{1}{2}\left(\frac{P_{\theta_0}}{\rho} - \tfrac{1}{2}\rho\Omega\right)^2 + \tfrac{1}{2}\frac{\Omega_1^2(t)}{k^2} \\ &+ P_\rho \frac{\Omega_1(t)}{k} \cos(\theta_0 + \varsigma(t)) - \left(\frac{P_{\theta_0}}{\rho} - \tfrac{1}{2}\rho\Omega\right)\frac{\Omega_1(t)}{k} \sin(\theta_0 + \varsigma(t)). \end{aligned} \tag{14}$$

Since Z does not appear in H in Eq. (14), we conclude that P_Z given by Eq. (13c) is the constant of motion corresponding to the helical symmetry of the system. We might refer to the constancy of $p_z + k(xp_y - yp_x)$ as conservation of canonical "helical momentum," in analogy to canonical angular momentum, which is conserved in cylindrically symmetric systems. Using the definition of $\mathbf{p}$ and our choice of $\mathbf{A}$ given by Eqs. (7), we find

$$P_Z = v_z + kx\left(v_y + \frac{x\Omega}{2} - \frac{\Omega_y(z,t)}{k}\right) - ky\left(v_x - \frac{y\Omega}{2} - \frac{\Omega_x(z,t)}{k}\right). \tag{15}$$

Elimination of x and y in favor of the other two constants X and Y yields

$$P_Z = v_z + \frac{k}{2\Omega}\left[X^2\Omega^2 - \left(v_y - \frac{\Omega_y(z,t)}{k}\right)^2\right] + \frac{k}{2\Omega}\left[Y^2\Omega^2 - \left(v_x - \frac{\Omega_x(z,t)}{k}\right)^2\right]. \tag{16}$$

Equation (16) then allows us to write the constant corresponding to helical symmetry in the following useful form, independent of the trivally ignorable coordinates x and y:

$$C \equiv -\frac{\Omega}{k}P_Z + \tfrac{1}{2}\Omega^2(X^2 + Y^2) = -\frac{\Omega v_z}{k} + \tfrac{1}{2}\left(v_x - \frac{\Omega_x(z,t)}{k}\right)^2 + \tfrac{1}{2}\left(v_y - \frac{\Omega_y(z,t)}{k}\right)^2. \tag{17}$$

This constant in various approximations has been discovered previously by several researchers [1-5]; however the full generality of systems for which this quantity is exactly conserved and its connection with helical symmetry are generally not recognized.

While the Hamiltonian in Eq. (14) reflects a reduction of the dimensionality of the problem by one canonical pair, it does not lend itself conveniently to further analysis due to its continued dependence on transverse coordinates, which we know to be trivially ignorable. To construct a Hamiltonian formally independent of X, Y, C, and C's canonical conjugate, q_C, it is easiest to return to Eq. (8). Using a procedure suggested by G. R. Smith[7,8] we perform a canonical transformation on the transverse coordinates: $(x, y, p_x, p_y) \rightarrow (X, Y, p_\phi, \phi)$ defined by:

$$(2\Omega p_\phi)^{1/2} \cos\phi = p_y - \tfrac{1}{2}x\Omega, \tag{18a}$$

$$(2\Omega p_\phi)^{1/2} \sin\phi = p_x + \tfrac{1}{2}y\Omega, \tag{18b}$$

$$\Omega X = p_y + \tfrac{1}{2}x\Omega, \tag{18c}$$

$$-\Omega Y = p_x - \tfrac{1}{2}y\Omega. \tag{18d}$$

The transformation may be verified to be canonical by taking Poisson brackets: $[\phi, p_\phi] = 1$, $\Omega[Y, X] = 1$, with all other Poisson brackets among the new coordinates vanishing. Note that the expressions for X and Y coincide with earlier definitions given by Eqs. (6) and (4). The new Hamiltonian under this transformation is

$$H = \tfrac{1}{2}p_z^2 + \Omega p_\phi + \tfrac{1}{2}\frac{\Omega_1^2(t)}{k^2} + (2\Omega p_\phi)^{1/2}\frac{\Omega_1(t)}{k}\sin(kz + \phi - \varsigma(t)). \tag{19}$$

As expected X and Y fail to appear, implying as before that both are constants of the motion. A final transformation, suggested by the Hamiltonian's dependence on z and ϕ only through the combination $kz + \phi - \varsigma(t)$, is defined by the generating function

$$F_2(z, \phi, p, C) = \left(z + \frac{\phi}{k} - \frac{\varsigma(t)}{k} + \frac{\pi}{2k}\right)\left(p + \frac{\omega(t) - \Omega}{k}\right) + \frac{\phi C}{\Omega}, \tag{20}$$

where $\omega(t) \equiv d\varsigma/dt$. The new generalized coordinates are given by

$$q = z + \frac{1}{k}\left(\phi - \varsigma(t) + \frac{\pi}{2}\right), \tag{21a}$$

$$p = p_z - \frac{\omega(t) - \Omega}{k}, \tag{21b}$$

$$q_C = \frac{\phi}{\Omega}, \tag{21c}$$

$$C = -\frac{\Omega p_z}{k} + \Omega p_\phi, \tag{21d}$$

where (q, p) and (q_C, C) are the conjugate pairs. Again note that C agrees with its previous definition (Eq. (17)). The new Hamiltonian under this transformation is

$$\begin{aligned} K &= H + \frac{\partial F_2}{\partial t} \\ &= \tfrac{1}{2}p^2 - \frac{\Omega_1(t)}{k}\left\{2\left[\frac{\Omega}{k}\left(p + \frac{\omega(t) - \Omega}{k}\right) + C\right]\right\}^{1/2}\cos kq + \frac{q}{k}\frac{d\omega}{dt} + C, \end{aligned} \tag{22}$$

in which terms depending only t, having no effect on the dynamics, have been dropped. The coordinate q_C does not appear in K verifying that C is a constant of the motion. The particle motion is thus seen to be described by a one-dimensional, time-dependent Hamiltonian $K(q,p,t)$ and depends only parametrically on C.

In addition to the three constants X, Y, and C, which always exist in the system described by Eqs. (1), a fourth constant may also be present, depending on initial conditions and specific time-dependence of the system fields.

The fourth conserved quantity exists, for example, for the important class of systems for which both Ω_1 and ω are time-independent. Then the Hamiltonian K itself, having no dependence on t, is the conserved quantity. By writing Eq. (22) in terms of rectangular coordinates and velocities and using Eqs. (1), we find the constant may be expressed as

$$\mathcal{E} \equiv \tfrac{1}{2}\left(v_z - \frac{\omega}{k}\right)^2 + \tfrac{1}{2}(v_x^2 + v_y^2) = K + \text{const.} \tag{23}$$

Thus the particle kinetic energy in the wave frame is conserved, a well-known result. Physically, the particle energy is conserved because the electric field vanishes in the frame of reference moving with the phase velocity of a constant amplitude, purely electromagnetic wave of fixed frequency.

We also find that an adiabatic invariant still exists when our assumptions are relaxed slightly to allow the field amplitude $\Omega_1(t)$ to be a slowly varying function of time. Consider for example those particle trajectories for which $p/P_0 \ll 1$, $kq \ll 1$, and $\omega_0^{-2} d\omega_0^2/dt \ll \omega_0$ where

$$P_0 \equiv \frac{\omega - \Omega}{k} + \frac{kC}{\Omega}, \tag{24a}$$

$$\omega_0^2(t) \equiv k^2 \frac{\Omega_1(t)}{k}\left(\frac{2\Omega P_0}{k}\right)^{1/2}. \tag{24b}$$

We will see shortly that these assumptions correspond to a deeply trapped particle moving in a wave whose amplitude varies slowly compared to the particle's trapping frequency ω_0. In terms of Eqs. (24), the Hamiltonian K may be expressed as

$$K = \tfrac{1}{2}p^2 - \epsilon^{-1}\frac{\omega_0^2(\epsilon t)}{k^2}\left(1 + \frac{\epsilon p}{P_0}\right)^{1/2} \cos(\epsilon^{1/2} kq) + \epsilon \frac{q}{k}\frac{d\omega}{dt}, \tag{25}$$

where ϵ may be considered a small parameter reflecting the ordering of our assumptions and will eventually be set equal to unity. (The additive constant C has been dropped from K for sake of clarity.) From the generating function

$$F_2(q,P,t) = \left(P + \frac{\omega_0^2(\epsilon t)}{2k^2 P_0}\right) q, \tag{26}$$

we obtain the canonical transformation

$$P = p - \frac{\omega_0^2(\epsilon t)}{2k^2 P_0}, \tag{27a}$$

$$Q = q, \tag{27b}$$

and the new Hamiltonian:

$$\begin{aligned}\mathcal{H} =& K + \frac{\partial F_2}{\partial t} \\ =& \tfrac{1}{2}\left(P + \frac{\omega_0^2}{2k^2 P_0}\right)^2 - \epsilon^{-1}\frac{\omega_0^2}{k^2}\left[1 + \frac{\epsilon}{P_0}\left(P + \frac{\omega_0^2}{2k^2 P_0}\right)\right]^{1/2} \cos(\epsilon^{1/2} kQ) \\ &+ \frac{\epsilon q \omega'}{k} + \frac{\epsilon \omega_0 \omega_0' Q}{k^2 P_0}. \end{aligned} \tag{28}$$

Expanding in powers of ϵ:

$$\begin{aligned}\mathcal{H} =& \tfrac{1}{2}P^2 + \tfrac{1}{2}\frac{\omega_0^2}{k^2 P_0}P + \frac{\omega_0^4}{8k^4 P_0^2} \\ &- \epsilon^{-1}\frac{\omega_0^2}{k^2}\left(1 + \frac{\epsilon P}{2P_0} + \frac{\epsilon\omega_0^2}{4P_0^2 k^2}\right)(1 - \tfrac{1}{2}\epsilon k^2 Q^2) + O(\epsilon) \\ \equiv& \mathcal{H}_{-1}\epsilon^{-1} + \mathcal{H}_0 \epsilon^0 + O(\epsilon). \end{aligned} \tag{29}$$

Since $\mathcal{H}_{-1}$ depends only on t, the effective Hamiltonian is given by $\mathcal{H}_0$ to lowest order. Dropping terms depending only on t, we find

$$\mathcal{H}_0(Q, P, t) = \tfrac{1}{2}P^2 + \tfrac{1}{2}\omega_0^2(\epsilon t)Q^2, \tag{30}$$

which is just the Hamiltonian for a simple harmonic oscillator with slowly varying frequency $\omega_0(\epsilon t)$. As with any such oscillator, the action defined by $\mathcal{H}_0(Q, P, t)$ is an adiabatic invariant to order ϵ^0. We are thus led to a fourth constant of the motion, existing within the adiabatic approximation, given to order ϵ^0 by

$$J \equiv \frac{\mathcal{H}_0}{\omega_0} = \frac{1}{2\omega_0}\left[\left(p - \frac{\omega_0^2}{2k^2 P_0}\right)^2 + \omega_0^2 q^2\right], \tag{31}$$

for particles whose orbits satisfy $kq \ll 1$, $p/P_0 \ll 1$.

III. FEATURES OF THE PARTICLE MOTION

The existence of the constants of motion derived here has a number of implications as regards the particle motion. Here we discuss : (1) accessible regions of velocity space, (2) particle trapping, and (3) slow time-scale motion of fixed points. Other features which should be explainable within our theory appeared in simulations; these are examined in Sec. IV.

The constant C given in Eq. (17) imposes severe restrictions on the motion of particles in $v_\perp$-v_z space. This is easily seen by expanding the quadratic terms in Eq. (17) and using the fact that $\Omega_x^2(z,t) + \Omega_y^2(z,t) = \Omega_1^2(t)$ from Eqs. (1). We obtain

$$C = -\frac{\Omega v_z}{k} + \tfrac{1}{2}v_\perp^2 - v_\perp \frac{\Omega_1(t)}{k}\cos\psi + \tfrac{1}{2}\frac{\Omega_1^2(t)}{k^2}, \tag{32}$$

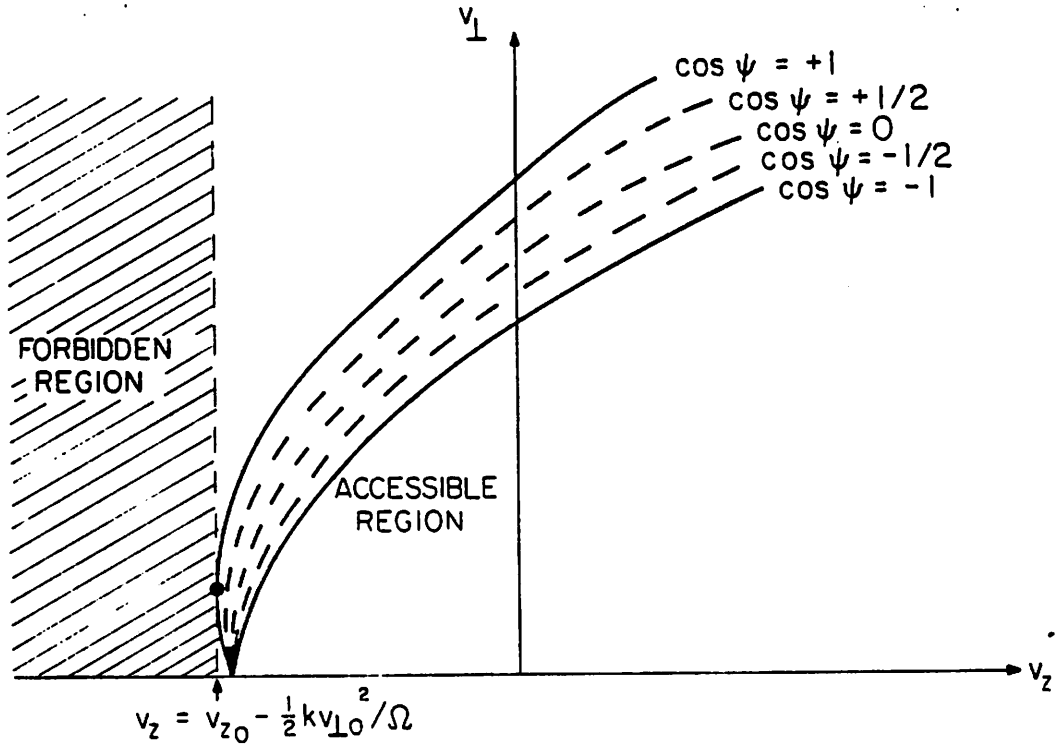

FIG. 2. Diagram depicting the region accessible to a particle with initial conditions $v_{\perp 0}$ and v_{z0} for a given wave amplitude Ω_1 and the region forbidden for any value of Ω_1. Also shown is the correspondence of points in the accessible region to selected values of $\cos\psi$, ψ being the angle between $\mathbf{v}_\perp$ and $\boldsymbol{\Omega}_\perp$.

where ψ is defined as the angle between $\mathbf{v}_\perp \equiv (v_x, v_y)$ and $\boldsymbol{\Omega}_\perp \equiv (\Omega_x, \Omega_y)$, i.e., $\mathbf{v}_\perp \cdot \boldsymbol{\Omega}_\perp = v_\perp \Omega_1(t) \cos\psi$.

Since it is often the case that the wave is vanishingly small as $t \to -\infty$, (in particular, this is true of our AIC simulations) we find it convenient to express C in terms of initial conditions:

$$C = \tfrac{1}{2} v_{\perp 0}^2 - \frac{\Omega}{k} v_{z0}, \tag{33}$$

where $v_{\perp 0} \equiv v_\perp(t \to -\infty)$ and $v_{z0} \equiv v_z(t \to -\infty)$. These definitions, but not the theory itself, make the assumption that $\Omega_1(t \to -\infty) = 0$.

Since $-1 \leq \cos\psi \leq 1$ it is immediately evident that a particle with initial velocities $v_{\perp 0}$ and v_{z0} will always satisfy:

$$-\frac{\Omega_1(t)}{\Omega} v_\perp \leq (v_z - v_{z0}) - \frac{k}{2\Omega}(v_\perp^2 - v_{\perp 0}^2) - \tfrac{1}{2}\frac{\Omega_1^2(t)}{k\Omega} \leq \frac{\Omega_1(t)}{\Omega} v_\perp. \tag{34}$$

This "accessible region" as a subset of $v_\perp$-v_z space is shown in Fig. 2. The particle will never leave this region irrespective of the wave's amplitude or time-dependence.

We note however that the location and extent of the region itself depends on the wave amplitude $\Omega_1(t)$. In the weak wave-field limit, particles are constrained to move on parabolas of the form

$$v_z = v_{z0} + \frac{k}{2\Omega}(v_\perp^2 - v_{\perp 0}^2). \tag{35}$$

This constraint is somewhat of a curiosity in view of the fact that in the many-wave counterpart of our system, quasilinear theory instead predicts transport along constant-$\mathcal{E}$ contours. In the presence of appreciable wave amplitudes $\Omega_1(t)$, the region exhibits some width and also moves to higher v_z due to the term quadratic in $\Omega_1(t)$ in Eq. (34). This motion of both the region and also its point of contact with the v_z-axis (i.e., $v_\perp = 0$) suggests that, with increasing wave amplitude, particles trapped in the region may also on average be transported to more positive values of v_z. A numerical study of particle orbits would likely be required to investigate the validity of this notion.

Also noteworthy is the fact that although the different regions of $v_\perp$-v_z space are accessible depending on the value of $\Omega_1(t)$, there exists a forbidden region which is never accessible irrespective of the magnitude of the wave amplitude. This result follows easily from Eq. (17):

$$-\frac{\Omega v_z}{k} \leq C = \tfrac{1}{2}v_{\perp 0}^2 - \frac{\Omega}{k}v_{z0}. \tag{36}$$

Thus the region $v_z < v_{z0} - \frac{1}{2}kv_{\perp 0}^2/\Omega$, shown in Fig. 2, will never be occupied by a particle with initial conditions $(v_{\perp 0}, v_{z0})$. Notice that the accessible region always maintains a point of tangency with the forbidden region. A particle occupying the point of tangency must have $v_x = \Omega_x(z,t)/k$, $v_y = \Omega_y(z,t)/k$, and $v_z = v_{z0} - \frac{1}{2}kv_{\perp 0}^2/\Omega$, or equivalently, must have $\cos\psi = 1$, $v_\perp = \Omega_1/k$, and $v_z = v_{z0} - \frac{1}{2}kv_{\perp 0}^2/\Omega$.

The simple dependence of C on ψ in Eq. (32) allows us to associate with various curves in the accessible region different values of $\cos\psi$. A few of these curves are shown in Fig. 2. The implication drawn is that a particle instantaneously found on a given curve must simultaneously exhibit the corresponding value of $\cos\psi$. This construct has an obvious realization in $v_\perp$-v_z-ψ space. The curves map into themselves in the larger space on constant-ψ sub-planes according to Eq. (32). The surface created by the union of these curves in $v_\perp$-v_z-ψ space is a constant-C surface on which particles with the appropriate value of C will forever be resident (although, again, the positioning of the surface is a function of $\Omega_1(t)$). The image of the projection of this surface into $v_\perp$-v_z space is, of course, the accessible region just described. A typical constant-C surface along with its projection are shown in Fig. 3.

The problem is thus reduced to the task of describing the particle motion on this constant-C surface. Discussion of this problem is facilitated by an examination of the structure of constant-$\mathcal{E}$ contours on the constant-C surface. In the case of a constant-amplitude, fixed-frequency wave, the role of the contours is obvious, since they must coincide with particle trajectories owing to the conservation of $\mathcal{E}$. They are also useful in describing particle motion in wave fields whose amplitude is slowly-varying, since in this case, it may be shown that the contours are level curves of the adiabatic invariant J to order ϵ^0. To the extent that the adiabatic assumption holds, the topology of these contours then characterizes

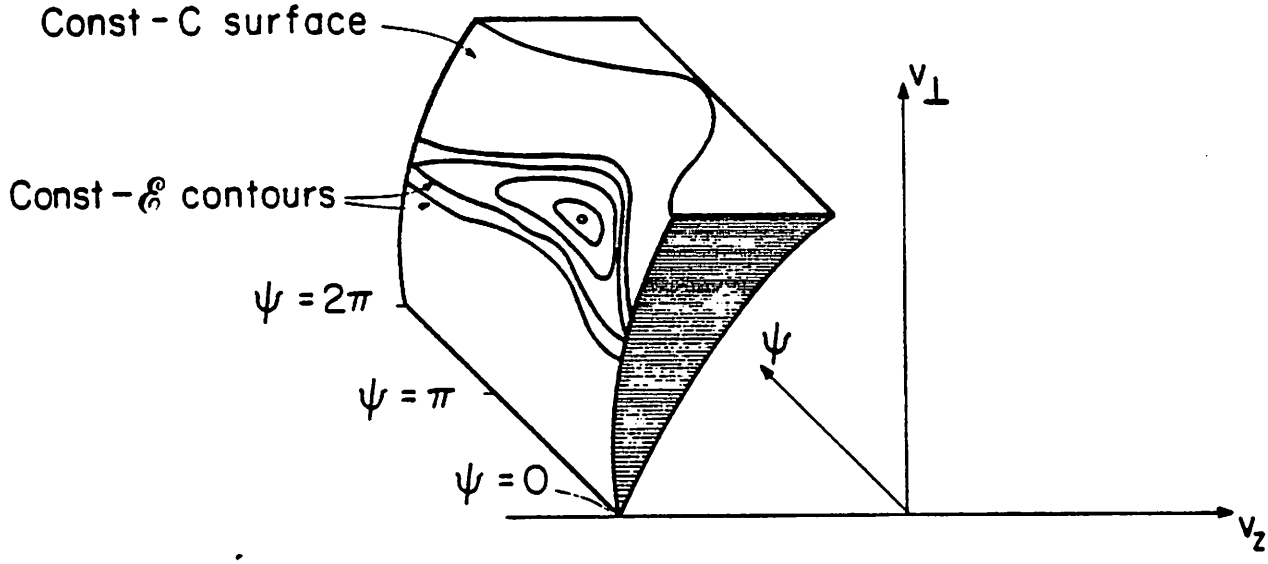

FIG. 3. Drawing of a typical constant-C surface in $v_\perp$-v_z-ψ space and its projection into $v_\perp$-v_z space (shaded region). Typical constant-$\mathcal{E}$ contours near the principal stable fixed point are also shown.

the behavior of the particles. Details of the particle orbits and the location, existence, and stability of fixed points have been described for a constant-amplitude wave by Bell.[9] Qualitative features of the arrangement of the contours on the constant-C surface may be determined geometrically as illustrated in Fig. 4. As an example, the point of tangency of a constant-$\mathcal{E}$ circle with a boundary of the accessible region and neighboring constant-$\mathcal{E}$ circles inside the region shown in Fig. 4 correspond respectively to a stable fixed point and its associated trapped particle contours as shown in Fig. 3.

While often as many as three fixed points exist on a constant-C surface, we will be primarily interested in the one residing on the $\cos\psi = -1$ boundary of the accessible region which will be referred to as the "principal" fixed point. We now detail the slow-time-scale motion of this fixed point and show that it is always stable.

For small wave amplitudes, v_z of the principal fixed point is approximately $(\omega - \Omega)/k$, which is generally thought of as the resonant velocity of the wave. However, as some authors have observed[3-5], in the presence of a finite amplitude wave, v_z of the fixed point shifts. The effect of this shift in the resonant velocity resembles that of a nonlinear frequency shift although in our case, the shift occurs even when the wave frequency ω remains constant. We can demonstrate the existence of the shift using three different approaches. The first has already been presented; from Eqs. (27) and (30) it is evident that the location of the bottom of the effective potential well is given by

$$p_{fp} = \frac{\omega_0^2}{2k^2 \mathcal{P}_0}, \tag{37a}$$

$$q_{fp} = 0, \tag{37b}$$

as long as $p_{fp} \ll \mathcal{P}_0$. It is easily shown from previous definitions that:

$$\mathcal{P}_0 = \frac{k}{2\Omega}\left[\left(v_\perp \cos\psi - \frac{\Omega_1(t)}{k}\right)^2 + v_\perp^2 \sin^2\psi - \frac{2\Omega}{k}\left(v_z - \frac{\omega - \Omega}{k}\right)\right], \tag{38}$$

$$\frac{\omega_0^2}{k^2} = \frac{\Omega_1(t)}{k}\left[\left(v_\perp \cos\psi - \frac{\Omega_1(t)}{k}\right)^2 + v_\perp^2 \sin^2\psi - \frac{2\Omega}{k}\left(v_z - \frac{\omega - \Omega}{k}\right)\right]^{1/2}, \tag{39}$$

$$p = v_z - \frac{\omega - \Omega}{k}, \tag{40}$$

$$\cos kq = -\frac{v_\perp \cos\psi - \Omega_1(t)/k}{\left((v_\perp \cos\psi - \Omega_1(t)/k)^2 + v_\perp^2 \sin^2\psi\right)^{1/2}}. \tag{41}$$

Equations (37b) and (41) immediately give the ψ-coordinate of the principal fixed point (assuming $v_\perp > \Omega_1/k$),

$$\psi_{fp} = \pi \pmod{2\pi}, \tag{42}$$

whereupon Eq. (37a) is easily evaluated :

$$(v_z)_{fp} \approx \frac{\omega - \Omega}{k} + \frac{\Omega_1(t)\Omega}{k^2 (v_\perp)_{fp}}, \tag{43}$$

where in addition to $p_{fp} \ll \mathcal{P}_0$ it has also been assumed that $\Omega_1/k(v_\perp)_{fp} \ll 1$.

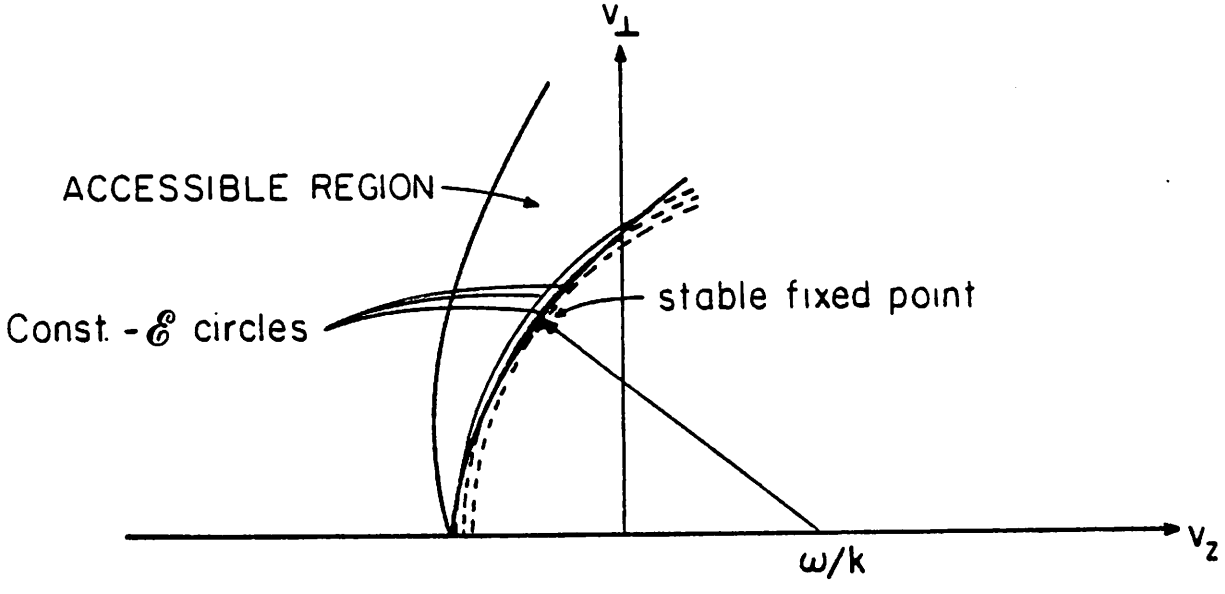

FIG. 4. Location of constant-$\mathcal{E}$ contours in the vicinity of a stable fixed point relative to a typical accessible region.

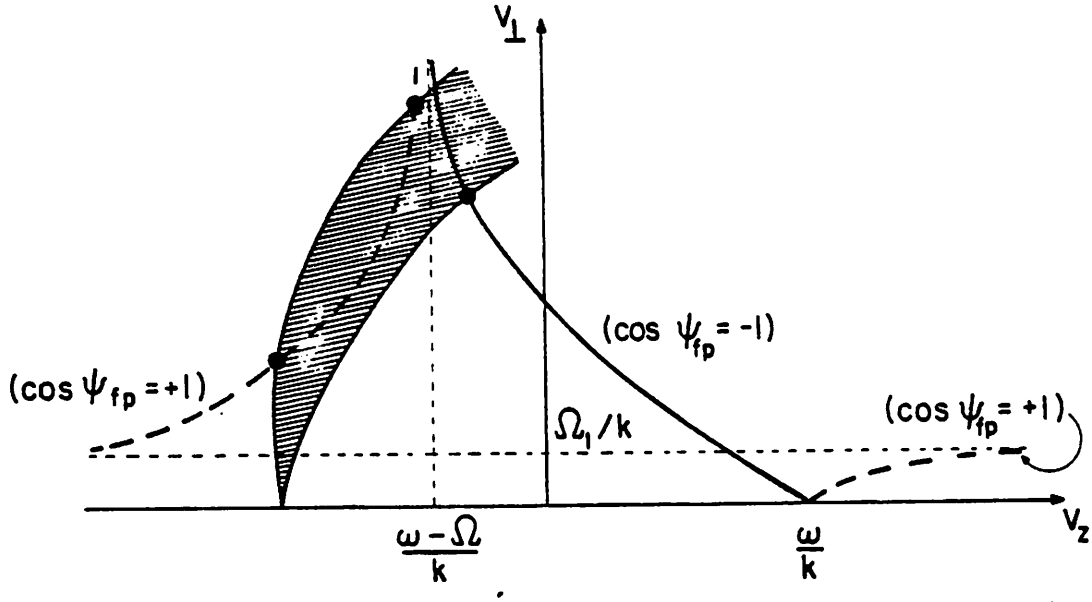

FIG. 5. Loci of fixed points for a fixed wave amplitude Ω_1. Fixed points having $\cos\psi_{fp} = -1$ lie along the solid curve; those with $\cos\psi_{fp} = +1$ reside on the dashed curves. Also shown are the fixed points ($\bullet$'s) and "accessible region" (shaded) for a typical value of the constant C.

The dependence of the location of the fixed point on the wave amplitude is also easily obtained directly from the equations of motion for a constant-amplitude single-frequency wave:

$$\dot{v_z} = \Omega_1 v_\perp \sin\psi, \tag{44a}$$

$$\dot{v_\perp} = \Omega_1 \left(\frac{\omega}{k} - v_z\right) \sin\psi, \tag{44b}$$

$$\dot{\psi} = kv_z - \omega + \Omega + \frac{\Omega_1}{v_\perp}\left(\frac{\omega}{k} - v_z\right)\cos\psi. \tag{44c}$$

From $\dot{v_z} = 0$ and $\dot{v_\perp} = 0$ we recover $\psi_{fp} = \pi$, which, combined with $\dot{\psi} = 0$ yields

$$(v_z)_{fp} = \frac{\omega}{k} - \frac{\Omega}{k}\frac{1}{1 + \Omega_1/k(v_\perp)_{fp}}. \tag{45}$$

which reduces to Eq. (43) for $\Omega_1/k(v_\perp)_{fp} \ll 1$. $\psi_{fp} = 0$ is also a solution to $\dot{v_z} = 0$ and $\dot{v_\perp} = 0$; in this case we find

$$(v_z)_{fp} = \frac{\omega}{k} - \frac{\Omega}{k}\frac{1}{1 - \Omega_1/k(v_\perp)_{fp}}. \tag{46}$$

The loci of fixed points described by these expressions are illustrated in Fig. 5.

A third perspective of the fixed point motion is suggested by Fig. 4. We expect the fixed points for a given value of C to appear as points of tangency between the constant-$\mathcal{E}$ circles and the $\cos\psi = -1$ boundary of the accessible region. The equation for this boundary is given by the right-hand equality in Eq. (34):

$$\frac{\Omega}{k}(v_z - v_{z0}) = \frac{1}{2}\left[\left(v_\perp + \frac{\Omega_1}{k}\right)^2 - v_{\perp 0}^2\right], \tag{47}$$

which may be differentiated to yield its slope:

$$\left.\frac{dv_\perp}{dv_z}\right|_{C,(\psi=\pi)} = \frac{\Omega}{k}\frac{1}{v_\perp + \Omega_1/k}. \tag{48}$$

Similarly, the slope of a constant-$\mathcal{E}$ circle, obtained from Eq. (23), is

$$\left.\frac{dv_\perp}{dv_z}\right|_{\mathcal{E}} = -\frac{v_z - \omega/k}{v_\perp}. \tag{49}$$

Equating the two slopes, we immediately obtain Eq. (45). We may also examine the stability of these fixed points by extending this method to the second derivatives:

$$\left.\frac{d^2v_\perp}{dv_z^2}\right|_{C,(\psi=\pi)} = -\frac{\Omega^2}{k^2}\frac{1}{(v_\perp + \Omega_1/k)^3}, \tag{50a}$$

$$\left.\frac{d^2v_\perp}{dv_z^2}\right|_{\mathcal{E}} = -\frac{v_\perp^2 + (v_z - \omega/k)^2}{v_\perp^3}. \tag{50b}$$

Equations (50a) and (50b) may be rearranged to yield

$$\left.\frac{d^2v_\perp}{dv_z^2}\right|_{\mathcal{E}} = \left.\frac{d^2v_\perp}{dv_z^2}\right|_{\psi,C}\left(1 + \frac{\Omega_1}{kv_\perp}\right)\left[1 + \frac{k^2}{\Omega^2}\left(v_\perp + \frac{\Omega_1}{k}\right)^2\right], \tag{51}$$

at the point of tangency. Since the factor on the right-hand side is always greater than unity and both second derivatives are negative definite, we may conclude that

$$\left.\frac{d^2v_\perp}{dv_z^2}\right|_{\mathcal{E}} < \left.\frac{d^2v_\perp}{dv_z^2}\right|_{\psi,C}, \tag{52}$$

at the fixed point on the $\cos\psi = -1$ boundary, for any value of C. As illustrated in Fig. 4, this condition implies that constant-$\mathcal{E}$ circles in the vicinity of the fixed point situated inside the accessible region must intersect the $\cos\psi = -1$ boundary on either side of the fixed point. This identifies the fixed point as stable; thus we have shown that any fixed point on the $\cos\psi = -1$ boundary is stable for any value of C.

The value of the $v_\perp$-coordinate of the fixed point $(v_\perp)_{fp}$ also depends on Ω_1 and is found by substituting Eq. (45) in Eq. (47):

$$\frac{\Omega}{k}\left(\frac{\omega}{k} - \frac{\Omega}{k}\frac{1}{1 + \Omega_1/k(v_\perp)_{fp}} - v_{z0}\right) = \frac{1}{2}\left[\left((v_\perp)_{fp} + \frac{\Omega_1}{k}\right)^2 - v_{\perp 0}^2\right]. \tag{53}$$

In the vanishing wave limit, we find

$$(v_\perp)_{fp}^2 \to v_{\perp 0}^2 + \frac{2\Omega}{k}\left(\frac{\omega-\Omega}{k} - v_{z0}\right) = \frac{2\Omega \mathcal{P}_0}{k} \equiv (v_{\perp 0})_{fp}^2 \qquad (\text{as } \Omega_1 \to 0), \tag{54}$$

$\mathcal{P}_0$ being defined in Eq. (24a). This expression is only valid for $\mathcal{P}_0 > 0$; when $\mathcal{P}_0 < 0$, $(v_{\perp 0})_{fp}^2 = 0$, as suggested by Fig. 5. Using this value of $(v_\perp)_{fp}$ in the terms involving Ω_1, we obtain for small wave amplitudes and $(v_{\perp 0})_{fp} \gg \Omega_1/k$:

$$(v_\perp)_{fp} \approx (v_{\perp 0})_{fp} - \frac{\Omega_1}{k(v_{\perp 0})_{fp}}\left(1 - \frac{\Omega^2}{k^2 (v_{\perp 0})_{fp}^2}\right). \tag{55}$$

It is clear that the principal fixed point may move to either lower or higher values of $v_\perp$ with increasing wave amplitude Ω_1. An exact expression for the direction of motion of $(v_\perp)_{fp}$ may be obtained by differentiating Eq. (53) by Ω_1:

$$k\frac{d(v_\perp)_{fp}}{d\Omega_1} = \frac{\Omega^2 k(v_\perp)_{fp} - (k(v_\perp)_{fp} + \Omega_1)^3}{\Omega^2 \Omega_1 + (k(v_\perp)_{fp} + \Omega_1)^3}. \tag{56}$$

Thus $(v_\perp)_{fp}$ increases with increasing Ω_1 when

$$\frac{k(v_\perp)_{fp}}{\Omega} > \left(\frac{k(v_\perp)_{fp} + \Omega_1}{\Omega}\right)^3. \tag{57}$$

Solutions to this inequality always lie in an interval subset of $0 < kv_\perp/\Omega < 1$. As $\Omega_1 \to 0$, the solution set approaches $(0, 1)$. For large enough Ω_1, $(\Omega_1 > 2/(3\sqrt{3})\Omega = 0.3849\Omega)$, the condition is never satisfied, and the value of $v_\perp$ decreases with increasing wave amplitude for all fixed points on the $\cos\psi = -1$ boundary of the accessible region.

IV. COMPARISON WITH AIC SIMULATIONS

Results of our single-wave theory were checked against data obtained from the particle-ion fluid-electron 1-d electromagnetic computer simulation code TRACY described in Appendix A. A single circularly-polarized spatial component of the wave fields was kept, with the time-dependence of the field allowed to be arbitrary. For ease of comparison, a simplified initial ion distribution was used. A small number of values of v_{z0} were chosen to represent a Maxwellian distribution in v_z, with all particles being loaded initially with the same value of $v_{\perp 0}$. For each $(v_{z0}, v_{\perp 0})$ pair, particles were loaded so as to uniformly fill both z-space and gyrophase space. This somewhat artificial distribution was chosen because both the fixed point motion, which is observed to depend on $v_{\perp 0}$, and features of the particle motion are more cleanly illustrated for this case. Meanwhile, the behavior of the wave-amplitude is identical in the linear growth stage, and qualitatively the same in the nonlinear stage, as the case of a full bimaxwellian distribution with the same values of $T_{i\|}$ and $T_{i\perp}$.

Several runs were conducted using various initial values of $v_{\perp 0}$ and $T_{i\|}$, with the run described here being typical. Parameters for this run were: $\Omega\Delta t = 0.038$, $v_A \Delta t/\Delta z = 0.31$, $N_p = 12032$, $N_b = 64$, $N_g = 256$, $\beta_{i\perp} = 2.0$, $T_{i\perp}/T_{i\|} = 4.0$, and $kv_A/\Omega = 0.795$. Here Δt

is the timestep size, Δz is the grid spacing, N_p is the number of simulation ion-particles, N_b is the number of values of v_{z0} loaded, N_g is the number of grid-points in the simulation system, and v_A is the Alfvén velocity $B_0/(4\pi n_0 m_i)^{1/2}$.

The code verified the invariance of C for particle motion in a single circularly-polarized wave field, conserving C to one part in 400 for several particles (Fig. 6) despite the rapid linear growth and nonlinear time-variation of the wave (Fig. 7). Existence of the "accessible region," a direct consequence of the invariance of C as explained in Sec. III, is also verified. Test particles initialized with identical values of $v_{\perp 0}$ and v_{z0} (i.e., identical values of C) but with different initial gyrophases ψ_0 remained within the "accessible region" through all stages of the simulation (Fig. 8).

The simulation also exhibited fixed point motion in good agreement with theory. As shown in Fig. 9, the behavior of the principal fixed point as determined by the cyclotron resonance condition bears qualitative resemblance to the simulation result when effects due to the nonlinear shift in the wave frequency are included (curve (b)). However, when the

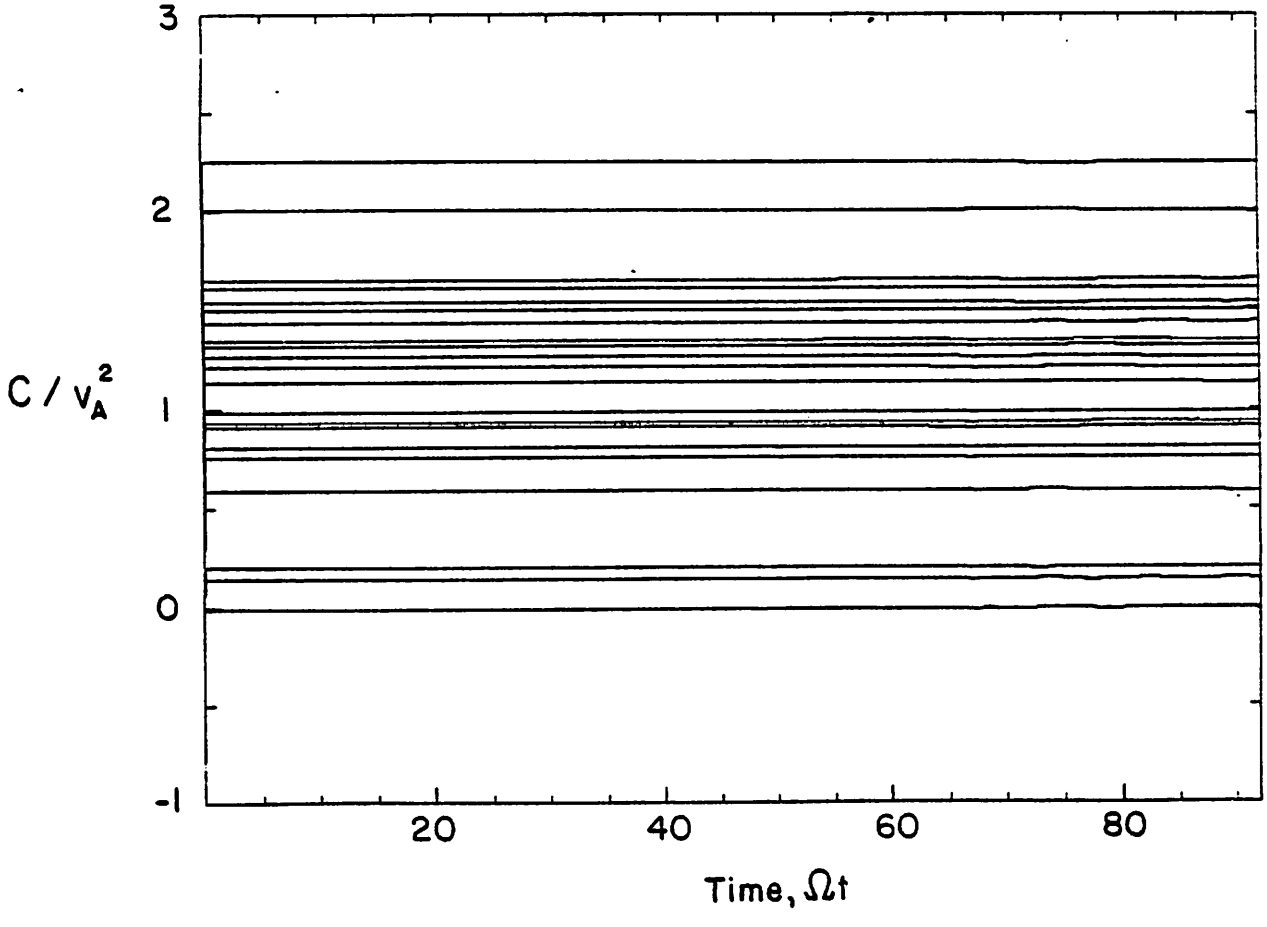

FIG. 6. Plot of C vs. time for particles with various initial conditions in a typical single-wave simulation.

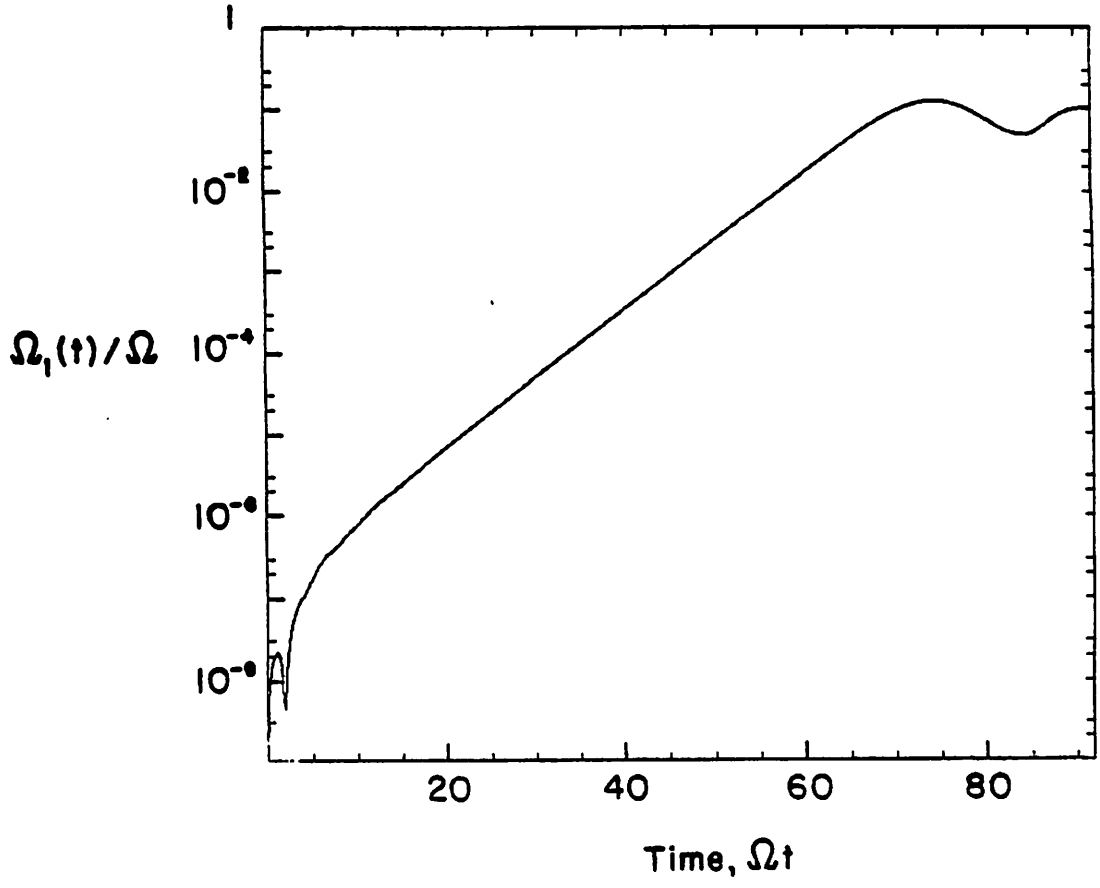

FIG. 7. Wave amplitude vs. time for a typical single-wave, single-$v_{\perp 0}$ AIC simulation run.

finite-wave correction is added (Eq. (43)), the resulting estimate (curve (c)) is considerably improved, tracking unexpectedly well with the simulation fixed point motion even though the underlying approximation, the adiabatic assumption, is at best only marginally satisfied. Thus our concepts of fixed points, trapping, action, etc. still appear to be meaningful in this regime, although in general we would not expect strict quantitative agreement with theory.

With the assumption that our understanding of fixed point characteristics is at least qualitatively correct, we next examine a striking effect observed in our single-wave, single-$v_{\perp 0}$ AIC simulations. The effect is illustrated in the series of snapshots displayed in Fig. 10. Figures 10(a) through 10(d) show the behavior of ion-particles as wave-saturation occurs (cf. Fig. 7). Comparison of Figs. 10(a) and 10(c) shows particle trapping by the wave and displacement of the v_z-coordinate of the fixed point $(v_z)_{fp}$ to more positive values (see also Fig. 9). Simultaneously, a very sharp "ridge" of high phase-space density forms "above" $(v_z > (v_z)_{fp})$ the fixed point and is clearly visible by the end of wave saturation

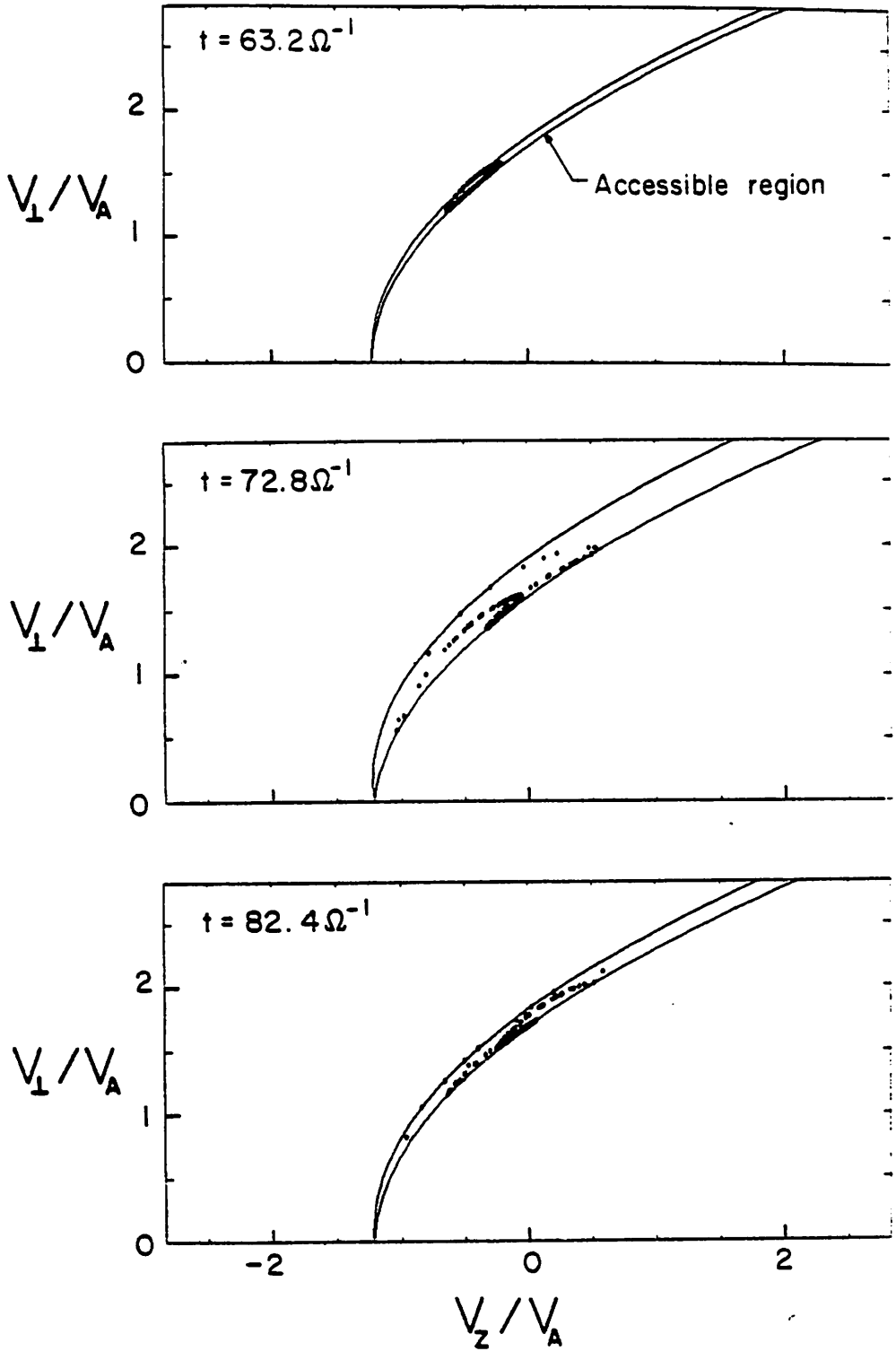

FIG. 8. Velocity-space locations of several simulation particles initialized with the same values of $v_{\perp 0}$ and v_{z0} relative to the theoretically-predicted "accessible region" at three different times.

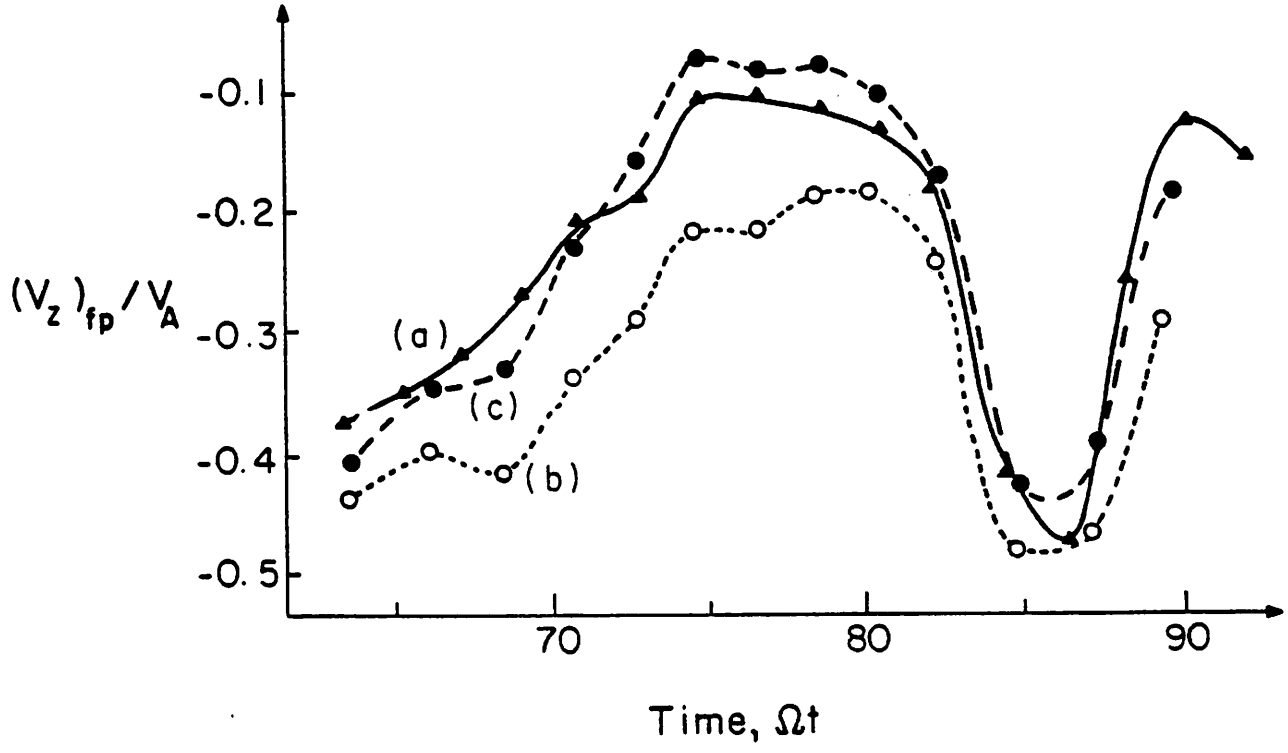

FIG. 9. Motion of the v_x-coordinate of the fixed point ($(v_x)_{fp}$) as observed in simulation and as calculated from two estimates : (a) simulated $(v_x)_{fp}/v_A$ vs. time, (b) $(\omega(t)-\Omega)/kv_A$ vs. time, (c) $(\omega(t)-\Omega)/kv_A + \Omega_1(t)\Omega/k^2(v_\perp)_{fp}v_A$ vs. time. Values for $(v_\perp)_{fp}$ ($= v_{\perp 0}$ independent of time), $\omega(t)$, and $\Omega_1(t)$ in (b) and (c) were obtained from the simulation.

(Fig. 10(c)). As the wave breaks, the ridge is swept to the underside of the fixed point (Fig. 10(e)) creating a density "edge" in velocity space most clearly seen in v_x-v_z (or v_y-v_z) space (Fig. 10(f)). After the wave has broken, the ridge structure is broken up by phase mixing (Fig. 10(g)) and the edge in velocity space loses definition (Fig. 10(h)).

Since the ridge appears only on one side of the fixed point (Fig. 10(c)), the cause must involve some factor asymmetric about the fixed point. This means that, for example, the standard comparison to particle trapping in the troughs of an electrostatic sinusoidal plane wave will not be sufficient to explain the effect, since phase space particle orbits in that case are symmetric with respect to the fixed point. We speculate that the formation of the ridge may be due to the motion of the fixed point to less negative values of v_z consistent with Eq. (43) and as seen in the simulation. Trapped particles in the path (i.e., $v_z > (v_z)_{fp}$) of the fixed point motion, attempting to conserve the action invariant J, may be piling up against particles less affected by the wave, producing the "ridge." Ridges might also be formed in the same manner simply because the wave is growing, since conservation of J demands that $\mathcal{H}_0$ increase as $\Omega_1^{1/2}$, displacing particles away from the fixed point. In this

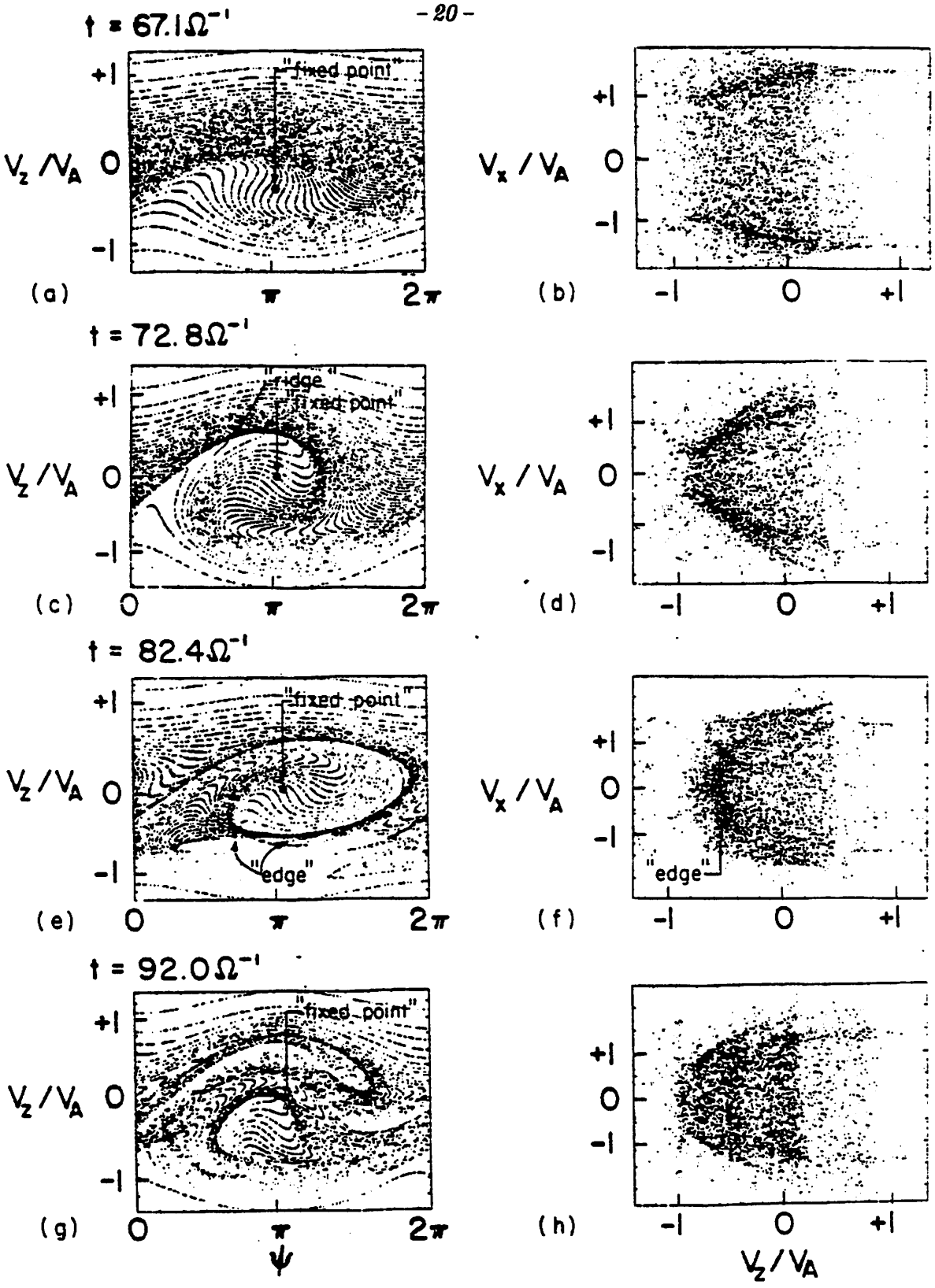

FIG. 10. Snapshots of the v_z/v_A vs. ψ and v_x/v_A vs. v_z/v_A ion phase spaces at four different times for a typical single-wave, single-$v_{\perp 0}$ AIC simulation.

case a ridge below the fixed point may also be visible, but likely less pronounced, than the ridge on top. Assuming this mechanism is operative, the density "edge" could result from the combined action of two effects: (1) particles trapped about the fixed point are transported with it to more positive v_z, leaving behind a lower density region below the eventual "ridge" location, and (2) half of a trapping libration brings the "ridge" around to the underside of the fixed point, where it coincides with the density "edge" boundary. This explanation needs further testing, but is consistent simulation data and is supported by the observed behavior of particles in a simulation movie of v_z-ψ phase space.

Finally, it is worth mentioning that, although all analysis conducted herein concerns the single-wave problem, some of our multiwave AIC simulations also show the formation of a less distinct, but unmistakable, edge in the velocity distribution. It may be the case that, although the quantity C is no longer conserved, the particle motion may retain some of the features of constant-C motion. In particular, particles may continue to exhibit a tendency to move to higher values of v_z with increasing wave amplitude, since both the accessible regions and the principal fixed points corresponding to each of the individual waves all move in the same direction. Again, definitive conclusions regarding the particle behavior in the multiwave case await further investigation.

V. CONCLUSIONS

Three exact constants of the motion have been found for particles moving in a single, circularly-polarized wave propagating along a uniform background magnetic field. The constant corresponding to the helical symmetry of the system fields, C, is of particular interest because it permanently restricts each particle to a relatively small region of $v_\perp$-v_z space which generally moves to higher v_z with increasing wave amplitude. Confinement of particles to one of these regions was verified in single-wave computer simulations of the Alfvén-ion-cyclotron instability. Existence of the three constants of motion reduces the problem to motion of the particle on a two-dimensional surface in $v_\perp$-v_z-ψ space. When the wave amplitude is slowly varying, the motion on this surface is characterized by the existence and slow time-scale motion of fixed points. At least one stable fixed point always exists and its deeply trapped particles exhibit an adiabatic invariant, namely, the action J. It is hypothesized that particle trapping, fixed point motion, and the existence of J may be responsible for the appearence of an edge in the v_z-distribution function shortly after wave saturation. The edge in the distribution function is also observed in some multiwave simulations, suggesting that some of the single-wave features of the particle motion may still be present even though the principal basis for the analysis, the conservation of C, is no longer valid.

ACKNOWLEDGMENTS

The author is grateful to G. R. Smith, C. K. Birdsall, and J. Lerner for their enlighening discussions and general encouragement. This work was supported by U. S. Department of Energy Contract No. DE-AT03-76ET53064. Computational facilities were provided by the National Magnetic Fusion Energy Computer Center.

APPENDIX A: THE SIMULATION ALGORITHM

Computer simulations for this study are based on a 1-d, periodic electromagnetic model employing particle ions immersed in an electron fluid. The algorithm used is similar, but not identical, to one described in Byers *et al.*[10] Each timestep ion velocities are advanced with the Boris method[11] using fields linearly weighted from a grid:

$$\frac{\mathbf{v}_i^{n+1/2} - \mathbf{v}_i^{n-1/2}}{\Delta t} = \frac{e}{m} \sum_j S(z_i - z_j^n) \left(\mathbf{E}_j^n + \frac{1}{2c} (\mathbf{v}_i^{n+1/2} + \mathbf{v}_i^{n-1/2}) \times \mathbf{B}_j^n \right), \tag{A1}$$

where n, i, and j are the timestep, particle, and grid indices respectively, Δt is the timestep size, m is the ion mass, and $S(z)$ is the usual particle-in-cell shape factor. Ion positions are then advanced one-half timestep :

$$z_i^{n+1/2} = z_i^n + \frac{1}{2} (v_z)_i^{n+1/2} \Delta t, \tag{A2}$$

and the ion current collected :

$$(\mathbf{J}_{ion})_j^{n+1/2} = \sum_i S(z_j - z_i^{n+1/2}) \mathbf{v}_{\perp i}^{n+1/2}, \tag{A3}$$

where $\mathbf{v}_\perp \equiv \mathbf{v} - \mathbf{v} \cdot \hat{\mathbf{z}} \hat{\mathbf{z}}$, $\hat{\mathbf{z}}$ being the direction of the uniform background magnetic field $\mathbf{B_0}$. The ion current and old vector potential are then Fourier-transformed in space: $(\mathbf{J}_{ion})_j^{n+1/2} \rightarrow (\tilde{\mathbf{J}}_{ion})_k^{n+1/2}$, $\mathbf{A}_j^n \rightarrow \tilde{\mathbf{A}}_k^n$ assuming periodic boundary conditions $k = 2\pi l / L$ where l is an integer and L is the system length. The new Fourier-transformed vector potential $\tilde{\mathbf{A}}_k^{n+1}$ is found from Ampere's Law using for the electrons a linear $\mathbf{E} \times \mathbf{B}$ fluid. Similarity of this form of Ampere's Law to Eq. (A1) suggests that we again make use of the Boris method:

$$\frac{4\pi n_0 e}{B_0 c} \frac{\tilde{\mathbf{A}}_k^{n+1} - \tilde{\mathbf{A}}_k^n}{\Delta t} \times \hat{\mathbf{z}} = \frac{k^2}{2} (\tilde{\mathbf{A}}_k^{n+1} + \tilde{\mathbf{A}}_k^n) - \frac{4\pi}{c} (\tilde{\mathbf{J}}_{ion})_k^{n+1/2}, \tag{A4}$$

thus inheriting the desirable properties of time-reversibility and exact mode-by-mode conservation of the wave energy in the absence of ion sources. The new wave magnetic field Fourier components are calculated next :

$$\tilde{\mathbf{B}}_k^{n+1} = -ik \tilde{\mathbf{A}}_k^{n+1} \times \hat{\mathbf{z}}, \tag{A5}$$

and, after inverse Fourier transforming $\tilde{\mathbf{B}}_k^{n+1} \rightarrow \mathbf{B}_j^{n+1}$, $\tilde{\mathbf{A}}_k^{n+1} \rightarrow \mathbf{A}_j^{n+1}$, the new electric field is found :

$$\frac{1}{2} (\mathbf{E}_j^{n+1} + \mathbf{E}_j^n) = -\frac{1}{c \Delta t} (\mathbf{A}_j^{n+1} - \mathbf{A}_j^n). \tag{A6}$$

Finally, the ion positions are advanced the other half-timestep,

$$z_i^{n+1} = z_i^{n+1/2} + \frac{1}{2} (v_z)_i^{n+1/2} \Delta t, \tag{A7}$$

completing the timestep loop.

We have found this algorithm conserves the total energy,

$$\sum_i \frac{mv_i^2}{2} + \sum_j \frac{|\mathbf{B}_j|^2}{8\pi}, \tag{A8}$$

to better than one part in 10^4 in the simulations presented.

In addition to the usual ion-cyclotron and whistler modes, the algorithm also exhibits an unphysical odd-even mode with frequency ω in the range $\tan(\omega\Delta t/2) = (\Omega\Delta t/2)^{-1}$. Both theory and simulation show the mode to be stable in a cold plasma when $v_A\Delta t/\Delta z$ is appreciably less than 1. We have found that the stable version of the mode is easily killed by setting $\mathbf{E}^{n+1}$ equal to $(\mathbf{E}^{n+1} + \mathbf{E}^n)/2$ for some timestep n early in the run. While used in the code, this timestep-averaging procedure is not generally required, since the mode is never important once the AIC-unstable wave has grown appreciably compared to initial wave amplitudes.

References

[1]C. S. Roberts and S. J. Buchsbaum, "Motion of a Charged Particle in a Constant Magnetic Field and a Transverse Electromagnetic Wave Propagating along the Field," Physical Review **135A**, 381 (1964).

[2]B. Sonnerup and S.-Y. Su, "Large Amplitude Whistler Waves in a Hot Collision-Free Plasma," Physics of Fluids **10**, 462 (1967).

[3]P. Palmadesso and G. Schmidt, "Collisional Damping of a Large Amplitude Whistler Wave," Physics of Fluids **14**, 1411 (1971).

[4]M. J. Laird and F. B. Knox, "Exact Solution for Charged Particle Trajectories in an Electromagnetic Field," Physics of Fluids **8**, 755 (1965).

[5]R. F. Lutomirski and R. N. Sudan, "Exact Nonlinear Electromagnetic Whistler Modes," Physical Review **147**, 156 (1966).

[6]H. Goldstein, *Classical Mechanics* (Addison-Wesley, Reading, Mass., 1965), Chap. 8.

[7]G. R. Smith, private communication.

[8]G. R. Smith and A. N. Kaufman, "Stochastic Acceleration by an Obliquely Propagating Wave—An Example of Overlapping Resonances," Physics of Fluids **21**, 2230 (1978).

[9]T. F. Bell, "Nonlinear Alfvén Waves in a Vlasov Plasma," Physics of Fluids **8**, 1829 (1965).

[10]J. A. Byers, B. I. Cohen, W. C. Condit, and J. D. Hanson, "Hybrid Simulations of Quasineutral Phenomena in Magnetized Plasma," Journal of Computational Physics **27**, 363 (1978).

[11]J. P. Boris, "Relativistic Plasma Simulation—Optimization of a Hybrid Code," in *Proceedings of the Fourth Conference on Numerical Simulation of Plasmas*, edited by J. P. Boris and R. Shanny (U. S. Government Printing Office, Washington, D. C., 1970), p. 3.